Minimal Nuclear Energy Density Functional

What do we really know about nuclear energy density functionals?

Aurel Bulgac
University of Washington, Seattle

Collaborators:

Michael McNeil Forbes - Washington State University and UW
Shi Jin - University of Washington
Nicolas Schunck - Lawrence Livermore National Laboratory
Rodrigo Navarro Perez - Lawrence Livermore National Laboratory (now at Ohio State University)

The most important formula in nuclear physics:

Bethe-Weizsäcker mass formula for 2375 nuclei (AME 2012) and A≥16 and masses determined with an accuracy ≤ 1 MeV.

a_v	a_s	a_I	a'_I	a_C	a'_C	δ	χ_E
−15.47	16.73	22.87	0	0.699	0	0	3.30
−15.49	16.78	22.91	0	0.700	0	12.29	3.18
−15.32	17.76	24.96	−22.60	0.767	−0.675	0	2.64
−15.34	17.80	25.01	−22.43	0.767	−0.661	11.46	2.50
−15.77	17.50	23.65	0	0.723	0	0	1.87
−15.46	18.29	25.72	−26.00	0.792	−0.773	0	1.53

AME 2012

SeaLL1 NEDF (extracted from calculated masses)

$$E(N,Z) = a_v A + a_s A^{2/3} + a_C \frac{Z^2}{A^{1/3}} + a'_C \frac{Z^2}{A^{2/3}} + a_I \frac{(N-Z)^2}{A} + a'_I \frac{(N-Z)^2}{A^{4/3}} + \Delta.$$

$$\Delta = \begin{cases} -\delta A^{-1/2} & \text{even-even nuclei,} \\ 0 & \text{odd nuclei,} \\ \delta A^{-1/2} & \text{odd-odd nuclei.} \end{cases}$$

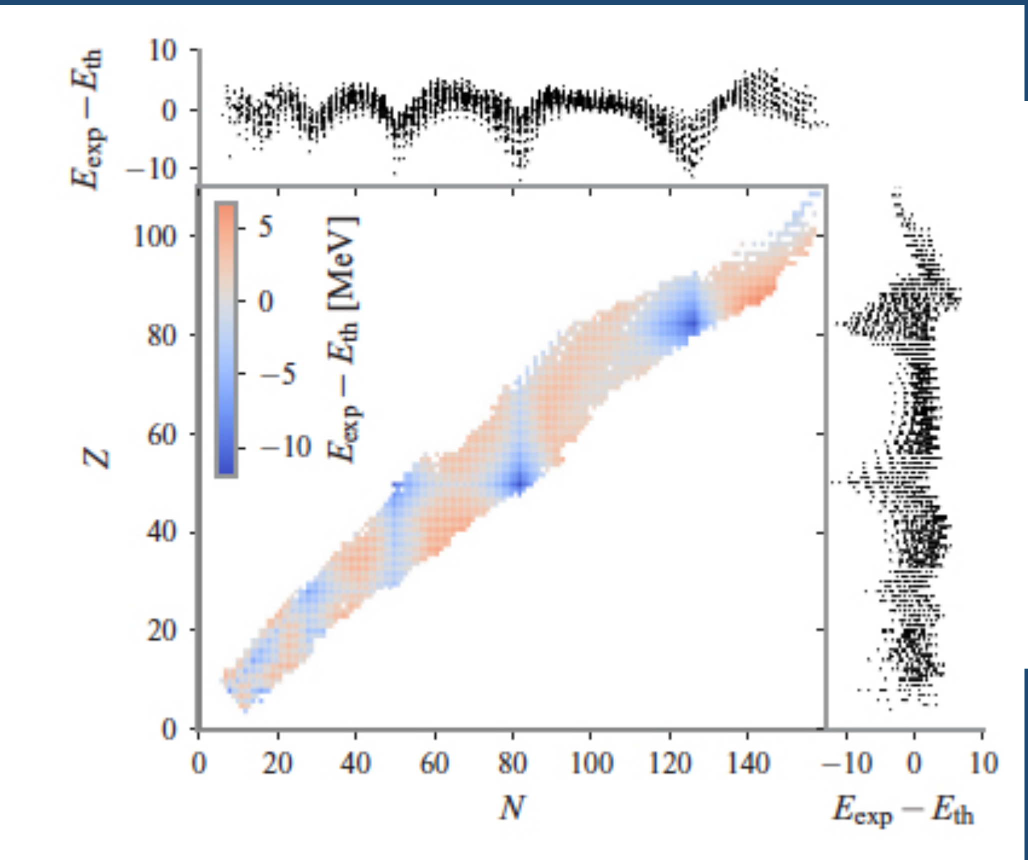

$E_{\rm exp} - E_{\rm th}$
$E_{\rm exp} - E_{\rm th}$ [MeV]
Z
N
$E_{\rm exp} - E_{\rm th}$

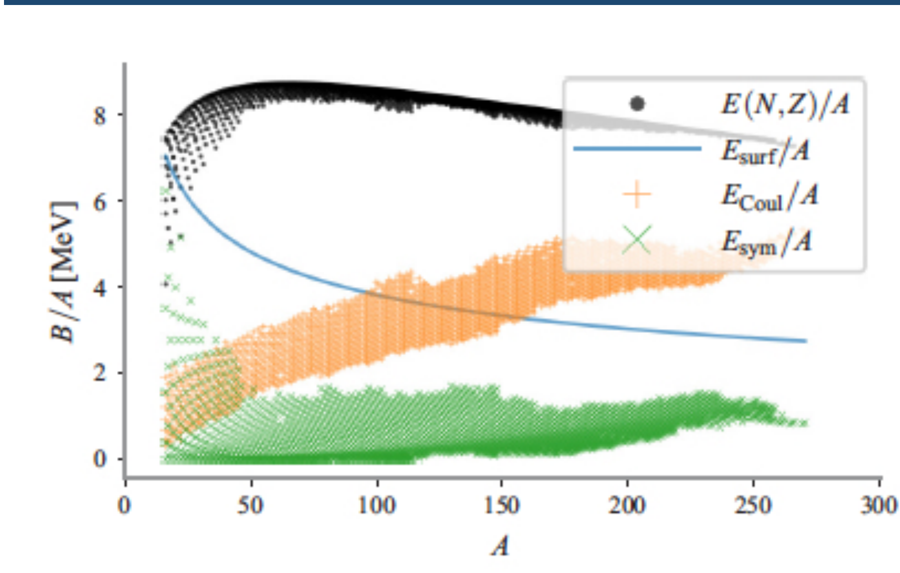

$E(N,Z)/A$
$E_{\rm surf}/A$
$E_{\rm Coul}/A$
$E_{\rm sym}/A$
B/A [MeV]
A

Single-particle density of states in a many-fermion system

$$E(A) = e_{TF} + A^{1/6}\,\#(\text{periodic orbits}) + 2.78\text{ MeV } A^{-1/3}$$
$$= e_{\text{vol}}V + e_{\text{surf}}S + \ldots + E_{\text{Coul}} + A^{1/6}\,\#(\text{periodic orbits})$$
$$+ 2.78\text{ MeV } A^{-1/3}\ \text{(quantum chaos)}$$

Supershells

$$\rho(\varepsilon) = \rho_{\text{TF}}(\varepsilon) + \rho_{\text{osc}}(\varepsilon),$$
$$\rho_{\text{osc}}(\varepsilon) = \sum_{\text{PO}} a_{\text{PO}}(\varepsilon)\sin\left(\frac{S_{\text{PO}}(\varepsilon)}{\hbar} + \phi_{\text{PO}}\frac{\pi}{2}\right) + \ldots$$
$$A = \int_{-\infty}^{\mu} \rho(\varepsilon)\,d\varepsilon, \qquad E_{\text{SC}} = \int_{-\infty}^{\mu} \varepsilon\,\rho_{\text{osc}}(\varepsilon)\,d\varepsilon.$$

Dominating periodic orbits (PO): triangle and square

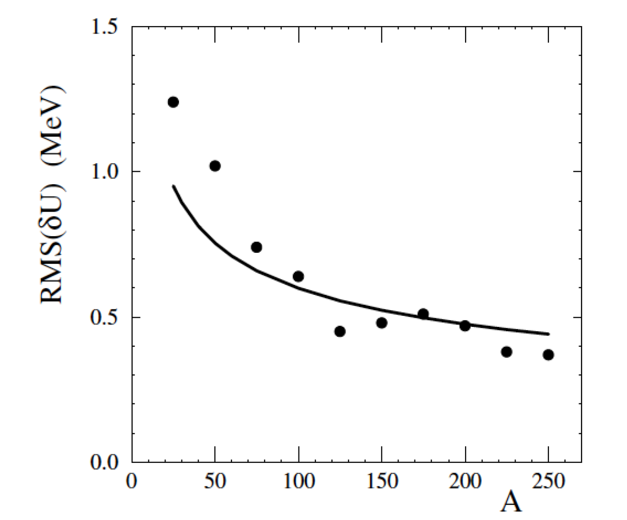

FIG. 1. RMS of the difference δU between computed and observed masses as a function of mass number A. Dots taken from Fig. 7 of Ref. [3], solid curve from Eq. (15).

Bohigas and Leboeuf
Phys. Rev. Lett. 88, 092502 (2002)

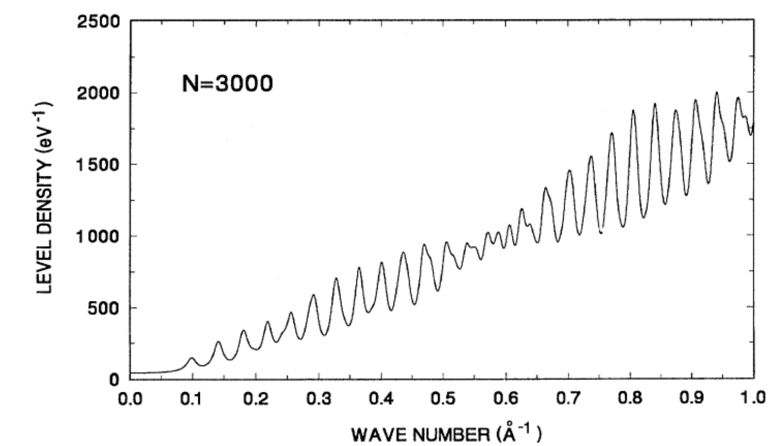

FIG. 10. Electronic single-particle level density $g(k)$ as a function of wave number k, evaluated in a spherical Woods-Saxon potential corresponding to a Na cluster with $N = 3000$, by Nishioka *et al.* (1990).

Theory: Balian and Bloch (1972), Berry and Tabor (1976), and Nishioka, Hansen, and Mottelson (1990).

Supershells have been observed in atomic clusters in 1980's

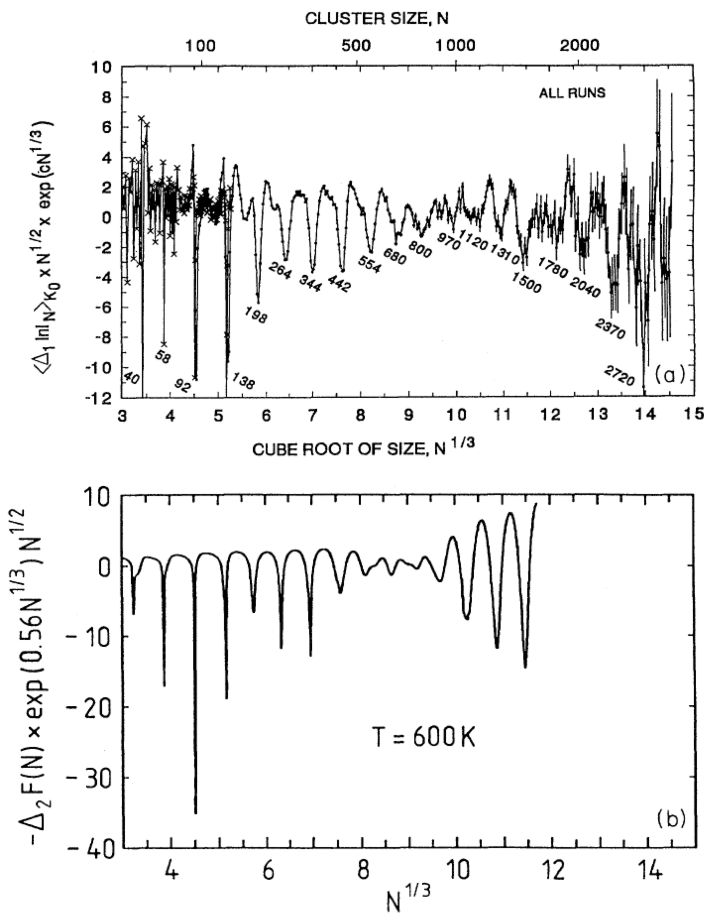

FIG. 12. Supershell beats in large sodium clusters: (a) Logarithmic derivative of the experimental mass yield of sodium clusters from an adiabatic expansion source, by Pedersen *et al.* (1991) (see this reference and the text for details); (b) second differences of total free energy obtained in self-consistent spherical jellium-Kohn-Sham-LDA calculations by Genzken and Brack (1991). See the text for an explanation of the exponential scaling factors.

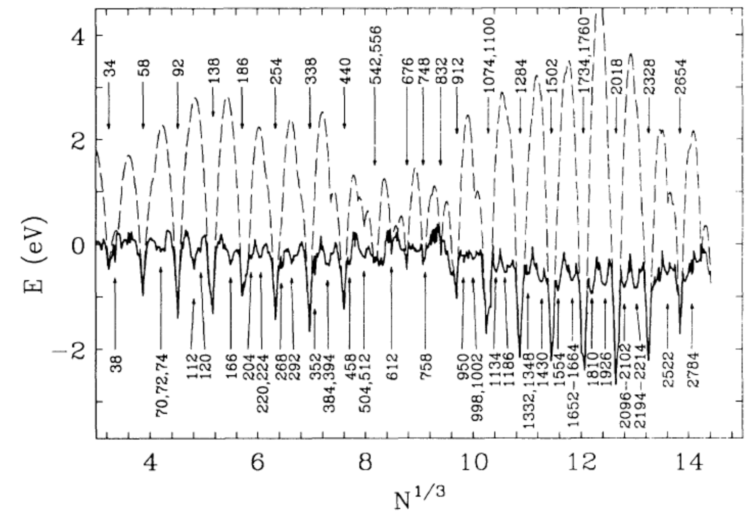

FIG. 1. The shell correction part of the total energy, determined for the most favorable configuration of a given cluster, solid line. The dashed line shows the same quantity computed for spherical geometry only. The numbers in the upper part of the plot designate the spherical magic numbers. The numbers in the lower part correspond to some of the most prominent minima of deformed clusters onlv.

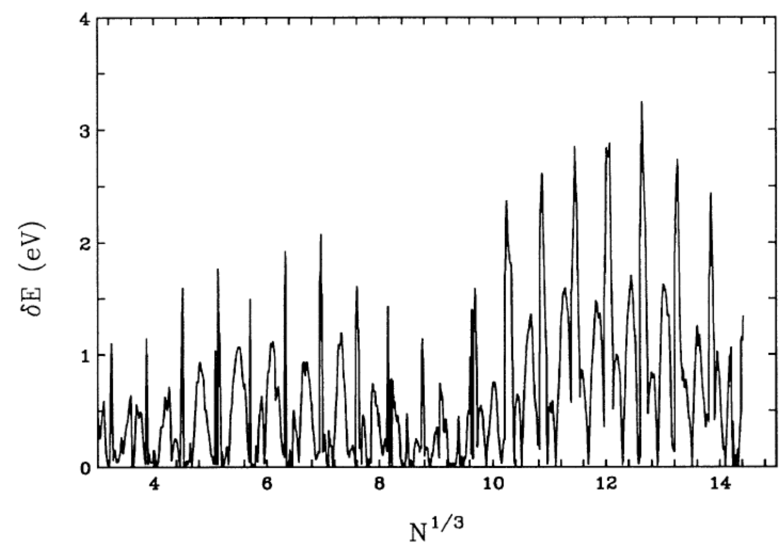

FIG. 4. The excitation energy of the first shape isomer of each cluster. The highest and sharpest peaks correspond to the spherical magic clusters.

S Bjørnholm et al (1990, 1991).

A (first) minimal nuclear energy density functional
SeaLL1

The full form of the functional SeaLL1 is

$$\mathcal{E}[n_n,n_p] = \overbrace{\frac{\hbar^2}{2m}(\tau_n+\tau_p)}^{\text{kinetic}} + \overbrace{\sum_{j=0}^{2}(a_j n^{5/3} + b_j n^2 + c_j n^{7/3})\beta^{2j}}^{\text{homogeneous}} + \overbrace{\eta_s \sum_{q=n,p} \frac{\hbar^2}{2m}|\nabla n_q|^2}^{\text{gradient}}$$
$$+ \underbrace{W_0 \boldsymbol{J}\cdot\nabla n}_{\text{spin-orbit}} + \underbrace{\sum_{q=n,p} g_{\text{eff}}(\boldsymbol{r})|\nu_q(\boldsymbol{r})|^2}_{\text{pairing}} + \underbrace{\frac{e^2}{2}\int d^3r' \frac{n_p(\boldsymbol{r})n_p(\boldsymbol{r}')}{|\boldsymbol{r}-\boldsymbol{r}'|} - \frac{e^2\pi}{4}\left[\frac{3n_p(\boldsymbol{r})}{\pi}\right]^{4/3}}_{\text{Coulomb}}.$$

- ✓ Terms not previously considered in literature proportional to $n^{5/3}$ and no powers higher than $n^{7/3}$!
- ✓ The apparent number of 9 (a,b,c's) + η_s+W_0+g_0 (volume pairing) = 12 parameters eventually comes down to <u>only seven parameters</u>!

- Semiclassical method (only four parameters), initially suggested by Weizsäcker (1935)

$$\mathcal{E}_{\text{kin}}[n_n,n_p] + \mathcal{E}_{\text{SO}}[n_n,n_p] = (\text{orbital-free})$$
$$= \frac{\hbar^2}{2m}\sum_{q=n,p}\tau_{\text{TF}}[n_q]F(X_q) - \frac{W_0^2}{2}\frac{2m}{\hbar^2}n|\nabla n|^2,$$

$$F(X) = \frac{1+(1+\kappa)X+9\kappa X^2}{1+\kappa X}, \quad X = \frac{\tau_2[n]}{\tau_{\text{TF}}[n]},$$
$$\tau_{\text{TF}}[n] = \frac{3}{5}(3\pi^2)^{2/3}n^{5/3}, \quad \tau_2[n] = \frac{1}{9}|\nabla\sqrt{n}|^2.$$

$$-\frac{\hbar^2}{2m}\nabla\left(\frac{F'(X_q)}{9}\nabla n_q^{1/2}\right) + U_q n_q^{1/2} = \mu_q n_q^{1/2},$$
$$U_q = \frac{\partial\mathcal{E}[n_n,n_p]}{\partial n_q}, \quad \text{for } q \in \{n,p\}.$$

- Using single-particle orbitals (seven parameters)

$$n = n_n + n_p, \qquad \beta = \frac{n_n - n_p}{n_n + n_p}.$$

Time-even densities

$$n(\boldsymbol{r}) = \sum_{k,\sigma} v_{k\sigma}^*(\boldsymbol{r})v_{k\sigma}(\boldsymbol{r}),$$
$$\nu(\boldsymbol{r}) = \sum_{k} v_{k\uparrow}^*(\boldsymbol{r})u_{k\downarrow}(\boldsymbol{r}),$$
$$\tau(\boldsymbol{r}) = \sum_{k,\sigma} \nabla v_{k\sigma}^*(\boldsymbol{r})\cdot\nabla v_{k\sigma}(\boldsymbol{r}),$$
$$\boldsymbol{J}(\boldsymbol{r}) = \frac{\nabla-\nabla'}{2\mathrm{i}} \times \sum_{k,\sigma,\sigma'} v_{k\sigma}^*(\boldsymbol{r})\boldsymbol{\sigma}_{\sigma,\sigma'}v_{k\sigma'}(\boldsymbol{r}')\bigg|_{\boldsymbol{r}=\boldsymbol{r}'}.$$

Time-odd densities

$$\boldsymbol{s}(\boldsymbol{r}) = \sum_{k,\sigma,\sigma'} v_{k\sigma}^*(\boldsymbol{r})\boldsymbol{\sigma}_{\sigma,\sigma'}v_{k\sigma'}(\boldsymbol{r}),$$
$$\boldsymbol{j}(\boldsymbol{r}) = \sum_{k,\sigma}\frac{\nabla-\nabla'}{2\mathrm{i}}v_{k\sigma}^*(\boldsymbol{r}')v_{k\sigma}(\boldsymbol{r})\bigg|_{\boldsymbol{r}=\boldsymbol{r}'};$$

Higher order corrections:

Higher order gradient corrections do not seem to be significant

$$\mathscr{E}_{\nabla^4}(\rho_n,\rho_p) = \sum_{\tau\in\{n,p\}} \frac{\hbar^2}{2m_\tau}\frac{1}{810(3\pi^2)^{2/3}} f(\rho_\tau), \qquad (13)$$

$$f(\rho) = \rho^{1/3}\left[\left(\frac{\nabla\rho}{\rho}\right)^4 - \frac{27}{8}\left(\frac{\nabla\rho}{\rho}\right)^2\frac{\nabla^2\rho}{\rho} + 3\left(\frac{\nabla^2\rho}{\rho}\right)^2\right].$$

Higher powers of the density ($n^{8/3}$, n^3,…) are not needed either!

- **How the fit was performed?**
- **What is the quality of other nuclear properties obtained without any further fitting?**

QMC of infinite homogeneous matter
(allows us to fix three parameters)

$$\mathcal{E}(n_n,n_p) = \frac{3\hbar^2(3\pi^2)^{2/3}}{10m}\left(n_n^{5/3}+n_p^{5/3}\right) + \sum_{j=0}^{2}(a_j n^{5/3} + b_j n^2 + c_j n^{7/3})\beta^{2j}.$$

Infinite homogeneous neutron matter (β=1)

$$\mathcal{E}_n(n_n) = \frac{3\hbar^2}{10m_n}(3\pi^2 n_n)^{2/3} n_n + \mathcal{E}_{\rm int}(n_n),$$
$$\mathcal{E}_{\rm int}(n_n) = a_n n_n^{5/3} + b_n n_n^2 + c_n n_n^{7/3},$$

Values fixed from QMC with chiral EFT 2N (N3LO) and 3N (N2LO) interactions

$$a_n = a_0 + a_1 + a_2 = -32.6\,\text{MeV fm}^2,$$
$$b_n = b_0 + b_1 + b_2 = -115.4\,\text{MeV fm}^3,$$
$$c_n = c_0 + c_1 + c_2 = 109.1\,\text{MeV fm}^4.$$

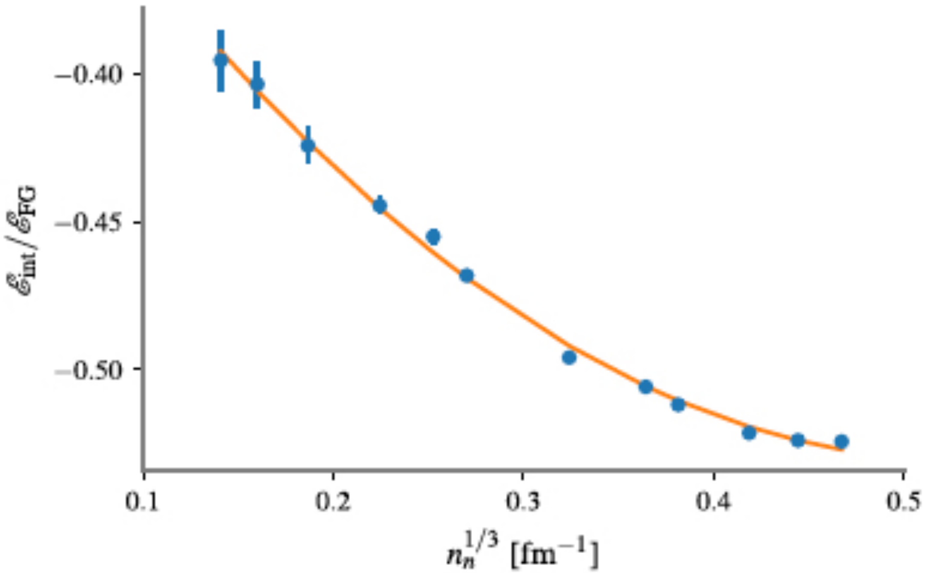

FIG. 3. The QMC results of Wlazłowski *et al.* [131] for the interaction energy per neutron displayed as the ratio $\mathcal{E}_{\rm int}/\mathcal{E}_{\rm FG}$ defined in Eq. (15b) (with $\beta = 1$), where $\mathcal{E}_{\rm FG} = 3\hbar^2(3\pi^2 n_n)^{2/3} n_n/(10 m_n)$. If $a_n = 0$ in Eq. (15b), the ratio $\mathcal{E}_{\rm int}/\mathcal{E}_{\rm FG}$ would tend to 0 for $n_n \to 0$. For densities $n_n^{1/3}|a_{nn}| < 1$ (where $a_{nn} = -18.9$ fm is the s-wave neutron-neutron scattering length), the leading-order correction to the kinetic energy density per particle contribution would be instead linear in density $4\pi\hbar^2 a_{nn} n_n/m_n$.

The term proportional to $n^{5/3}$ is clearly present, as in the case of the unitary Fermi gas!

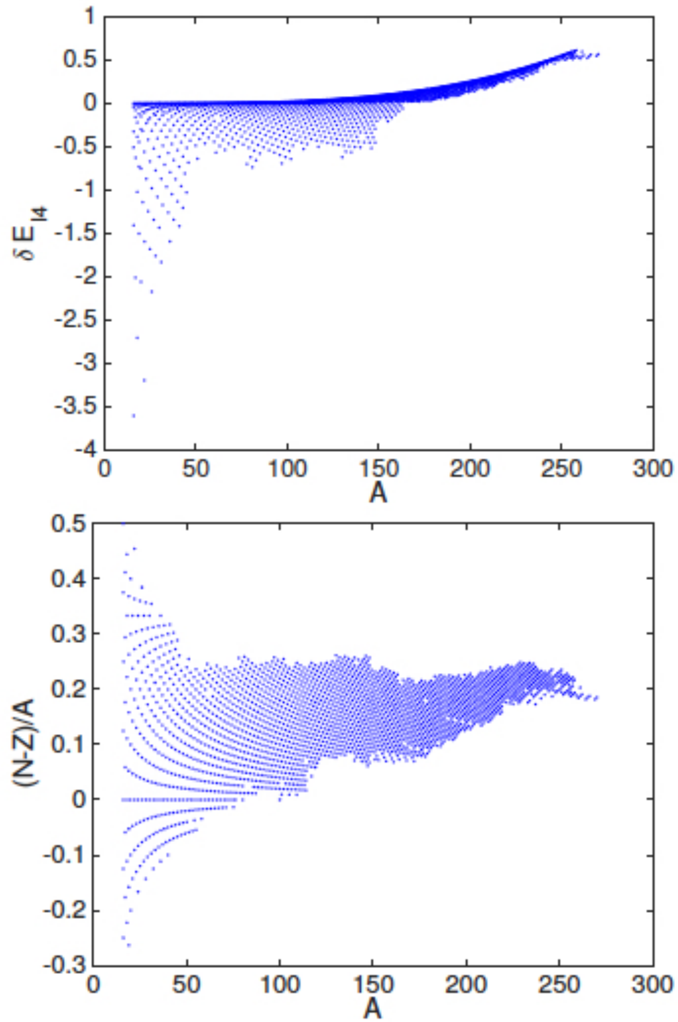

Figure 5 (Color online) The contribution to the ground state energies of the terms quartic in isospin density $\delta E_{I4} = \int d^3 \mathscr{E}_2(\rho)\beta^4$, evaluated perturbatively with NEDF-1, see Table II. In the lower panel we display the ratio $(N-Z)/A$ for the nuclei we have considered. Among the 2375 nuclei we have considered, there are 33 nuclei with $N = Z$, 78 nuclei with $Z > N$, and 70 nuclei with $|N-Z|/A > 1/4$.

$(N\text{-}Z)^4$ contributions to finite nuclei are rather small

TABLE II. Best-fit parameters for the SeaLL1 functional and the orbital-free approximation (next column in italic when different). The errors quoted for the fit parameters should be interpreted as estimating by how much this parameter can be independently changed while refitting the other and incurring a cost of at most $\delta\chi_E < 0.1$ MeV.

	SSeaLL1	Hydro	Comments
n_0	0.154	*0.154*	Adjusted (see Fig. 5)
a_0	0	Same	Insignificant
b_0	−684.5(10)	*−685.6(2)*	
c_0	827.26	*828.76*	$2c_0 n_0^{\frac{2}{3}} = -\frac{3\hbar^2}{10m}(\frac{3\pi^2}{2})^{\frac{2}{3}} - \frac{3}{2}b_0 n_0^{\frac{1}{3}}$
a_1	64.3	*50.9*	$a_1 = n_0^{1/3} b_1$
b_1	119.9(61)	*94.9(14)*	
c_1	−256(25)	*−160.0*	Fixed in orbital-free theory
a_2	−96.8	*−83.5*	$a_2 = a_n - a_0 - a_1$
b_2	449.2	*475.2*	$b_2 = b_n - b_0 - b_1$
c_2	−461.7	*559.6*	$c_2 = c_n - c_0 - c_1$
a_n	−32.6	Same	From neutron matter EoS (16)
b_n	−115.4	Same	From neutron matter EoS (16)
c_n	109.1	Same	From neutron matter EoS (16)
η_s	3.93(15)	*3.370(50)*	
W_0	73.5(52)	*0.0*	Fixed in orbital-free theory
g_0	−200	N/A	g_0 fit in Ref. [145]
κ	N/A	*0.2*	Semiclassical (see Sec. III H)
$\frac{\hbar^2}{2m}$	20.7355	Same	Units (MeV = fm = 1)
e^2	1.43996	Same	cgs units ($4\pi\epsilon_0 = 1$)
χ_E	1.74	*3.04*	606 even-even nuclei
		2.86	2375 nuclei
χ_r	0.034	*0.038*	345 charge radii
		0.041	883 charge radii

- In the orbital free framework there are four independent parameters: a_0, b_0, b_1, η_s.
- Using single-particle orbitals there are seven independent parameters: a_0, b_0, b_1, c_1, W_0, η_s, and g_0.

These parameters are fixed by

- ✓ Nuclear saturation density
- ✓ Binding energies of nuclei
- ✓ Symmetry energy and its density dependence
- ✓ Surface tension
- ✓ Spin-orbit strength
- ✓ Strength of pairing correlations

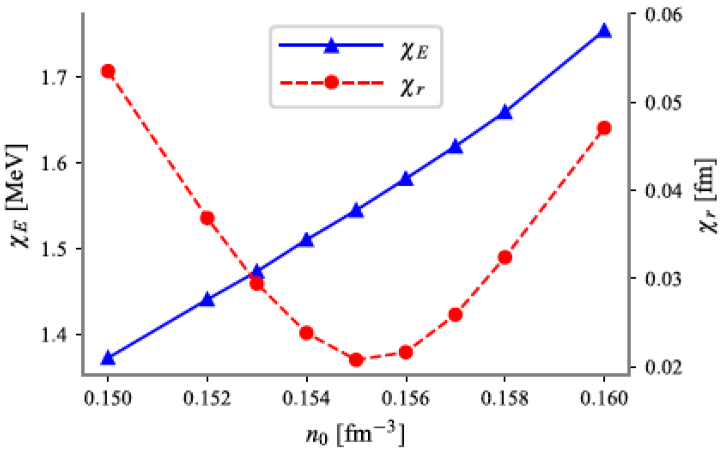

FIG. 5. Saturation density n_0 dependence of the energy residual χ_E and charge radii residual χ_r of the SeaLL1 functional. After holding n_0 fixed (through the parameter c_0), the remaining five shaded parameters in Table II were fit by minimizing only $\chi_E^2 = \sum |E_{N,Z} - E(N,Z)|^2/N_E$ over the $N_E = 196$ spherical even-even nuclei with $A \geqslant 16$ measured (not extrapolated) from Audi *et al.* [18], Wang *et al.* [19]. The value $n_0 = 0.154\,\mathrm{fm}^{-3}$ fixed in the SeaLL1 functional represents a compromise between these residuals here both χ_E and χ_r increase by about 10%.

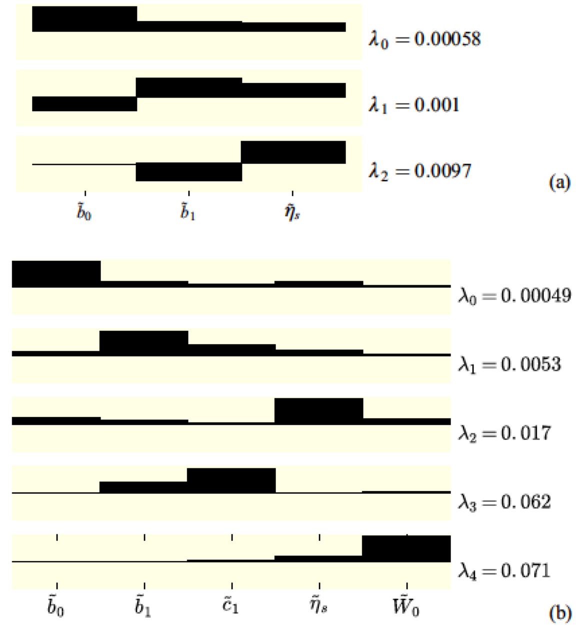

FIG. 6. The principal component analysis of the SeaLL1 NEDF in the case of the orbital-free (a) and orbital-based (b) approach.

$$p_n = v_n(\tilde{a}_0\ \tilde{b}_0\ \dots\ \tilde{\eta}_s\ \tilde{W}_0).$$

$$\tilde{a}_j = \frac{a_j n_0^{2/3}}{\varepsilon_F}, \quad \tilde{b}_j = \frac{b_j n_0}{\varepsilon_F}, \quad \tilde{c}_j = \frac{a_j n_0^{4/3}}{\varepsilon_F}.$$

$$\frac{\delta(\chi_E^2)}{2\chi_E \times 0.1\,\mathrm{MeV}} \approx \delta^T C^{-1} \delta = \sum_n \frac{(\delta p_n)^2}{\lambda_n^2}.$$

$$\frac{\varepsilon_0}{\varepsilon_F} = +\frac{3}{5} + \tilde{a}_0 + \tilde{b}_0 + \tilde{c}_0,$$

$$0 = +\frac{3}{5} + \tilde{a}_0 + \frac{3}{2}\tilde{b}_0 + 2\tilde{c}_0,$$

$$\frac{K_0}{\varepsilon_F} = -\frac{6}{5} - 2\tilde{a}_0 + 4\tilde{c}_0,$$

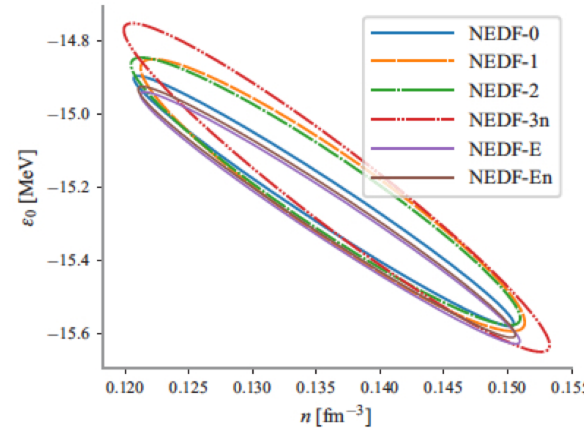

FIG. 21. The various ellipses show the region in the (ε_0, n_0) plane, in which the NEDF parameters can be changed and to lead to changes in the residual $\delta\chi_E < 0.2\,\mathrm{MeV}$. While the equilibrium energy ε_0 and density n_0 are controlled mainly by the combination $\tilde{b}_0 + \tilde{c}_0$, which is constrained with very high precision, the combination $\tilde{b}_0 - \tilde{c}_0$ has significantly less constraint; see Sec. III I. This aspect allows us to manipulate to a certain degree the saturation properties, while affecting the overall fit only slightly.

These do not contain quartic terms in β.

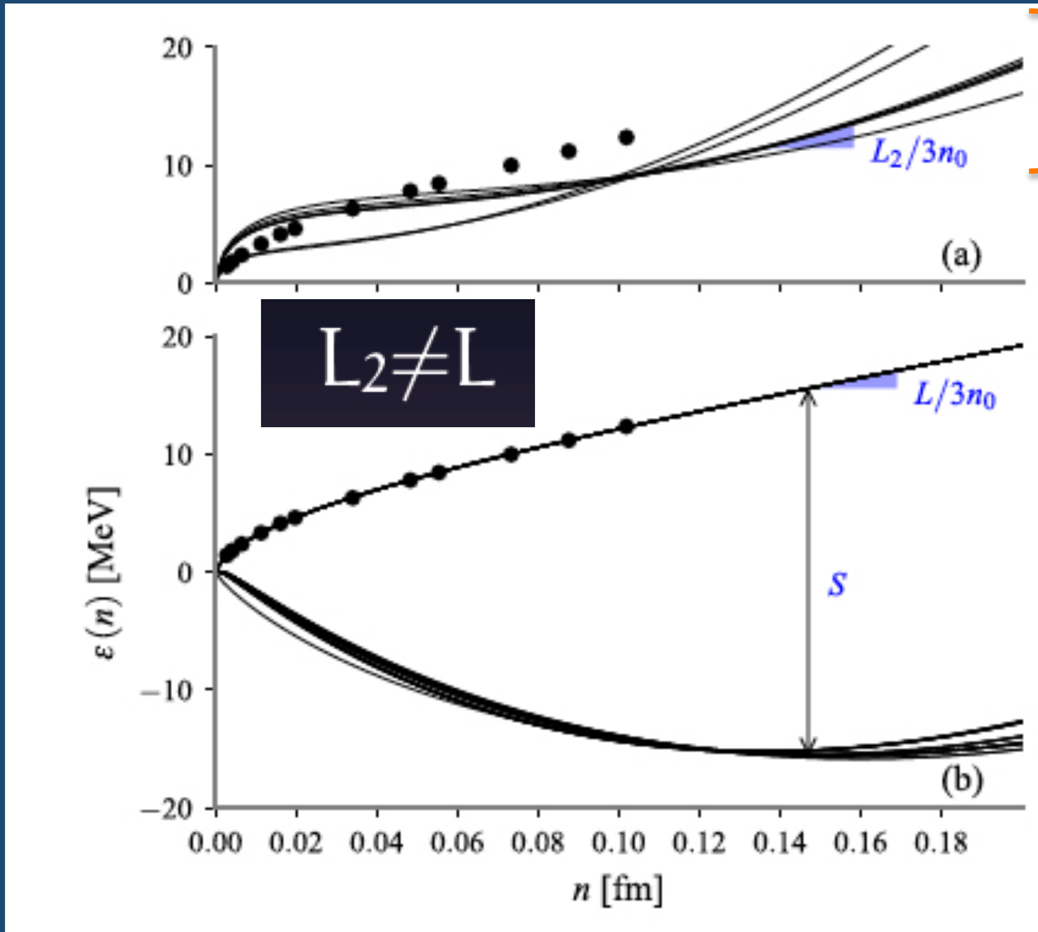

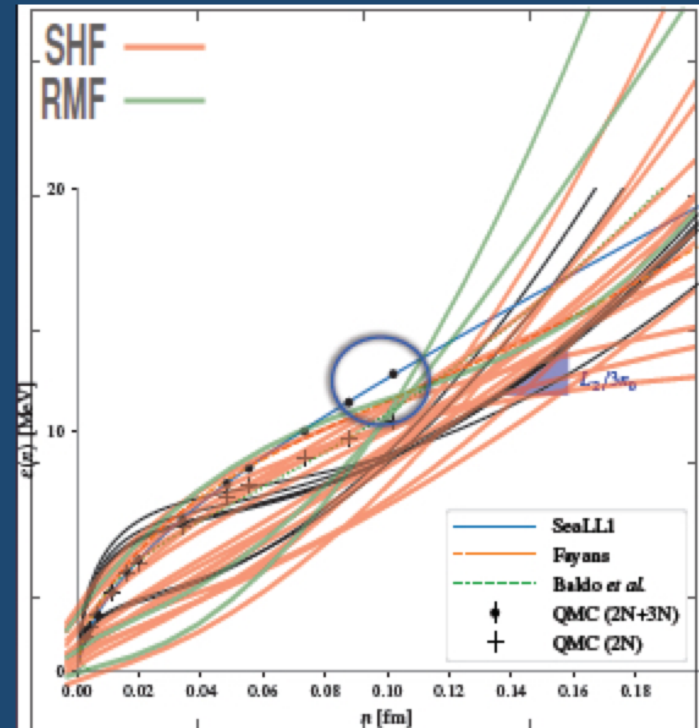

P.-G. Reinhard at ECT*, Trento, Italy, 26-30 January, 2015,
https://sites.google. com/site/ectworkshopns2015/talks

$$\mathscr{E}(\rho_n,\rho_p) = \frac{3\hbar^2(3\pi^2)^{2/3}}{10m}(\rho_n^{5/3}+\rho_p^{5/3}) + \sum_{j=0}^{2}\left(a_j\rho^{5/3}+b_j\rho^2+c_j\rho^{7/3}\right)\beta^{2j},$$

$$\frac{\mathscr{E}(\rho_n,\rho_p)}{\rho} = \varepsilon_0(\rho)+\varepsilon_2(\rho)\beta^2+\varepsilon_4(\rho)\beta^4+\mathscr{O}(\beta^6).$$

$$S = \frac{\mathscr{E}(\rho_0,0)-\mathscr{E}(\rho_0/2,\rho_0/2)}{\rho_0},$$

$$L = 3\rho\frac{\mathrm{d}}{\mathrm{d}\rho}\left(\frac{\mathscr{E}(\rho,0)}{\rho}\right)\bigg|_{\rho_0} = 3\rho_0\varepsilon_n'(\rho_0).$$

$$\rho = \rho_n+\rho_p, \qquad \beta = \frac{\rho_n-\rho_p}{\rho_n+\rho_p}.$$

Saturation, symmetry energy, compressibility, and neutron skin thickness

$$S = \frac{\mathcal{E}(n_0,0) - \mathcal{E}(n_0/2,n_0/2)}{n_0},$$

$$L = 3n\frac{d}{dn}\left[\frac{\mathcal{E}(n,0)}{n}\right]\bigg|_{n_0} = 3n_0\varepsilon_n'(n_0)$$

$$= \frac{6}{5}\frac{\hbar^2}{2m}(3\pi^2 n_0)^{2/3} + 2a_n n_0^{2/3} + 3b_n n_0 + 4c_n n_0^{4/3}.$$

$$\frac{\mathcal{E}(n_n,n_p)}{n} = \epsilon_0(n) + \epsilon_2(n)\beta^2 + \epsilon_4(n)\beta^4 + O(\beta^6).$$

$$\epsilon_0(n) = \tfrac{6}{5}\varepsilon_F + a_0 n^{2/3} + b_0 n + c_0 n^{4/3}$$
$$= \varepsilon_0 + \tfrac{1}{2}K_0\delta^2 + O(\delta^3),$$
$$\epsilon_2(n) = -\tfrac{4}{15}\varepsilon_F + a_1 n^{2/3} + b_1 n + c_1 n^{4/3}$$
$$= S_2 + L_2\delta + \tfrac{1}{2}K_2\delta^2 + O(\delta^3),$$
$$\epsilon_4(n) = S_4 + L_4\delta + \tfrac{1}{2}K_4\delta^2 + O(\delta^3).$$

$$\delta = (n - n_0)/3n_0$$

TABLE III. Saturation, symmetry, and neutron skin properties for SeaLL1. All values in MeV unless otherwise specified.

ρ_0 [fm^{-3}]	$-\epsilon_0$	K_0	S	S_2	L	L_2	Neutron skin ^{208}Pb [fm]	Neutron skin ^{48}Ca [fm]
0.154	15.6	230	31.7	27.7	32.4	32	0.131	0.159

$$S_2 = \tfrac{1}{3}\varepsilon_F + 2a_1 n_0^{2/3} + c_1 n_0^{4/3},$$
$$L_2 = \tfrac{2}{3}\varepsilon_F + 5a_1 n_0^{2/3} + 4c_1 n_0^{4/3}.$$

S_2, L_2, and neutron skin radius can be controlled with a_1-$b_1 n_0^{1/3}$ and c_1 which are largely unconstrained in SeaLL1

By changing a_0 by δa_0=±20 MeV fm^2 and keeping saturation energy and density fixed one can change incompressibility K_0 by δK_0= ±23 MeV

Quartic terms in β are needed only if one constrains binding energies of nuclei and neutron matter EoS at the same time!

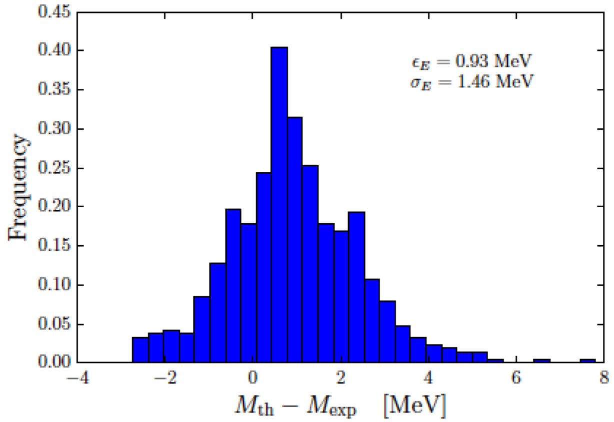

FIG. 9. The histogram of the mass residuals between SeaLL1 and experiment for 606 even-even nuclei.

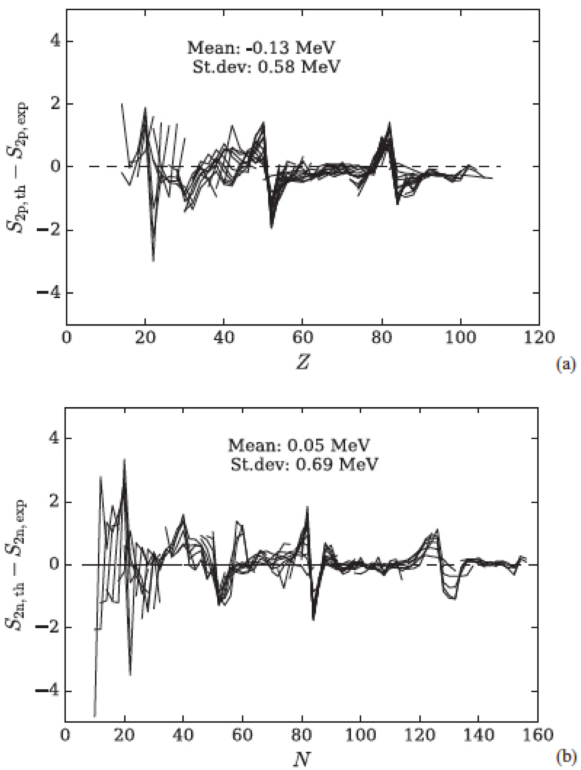

FIG. 10. The residual of the two-nucleon separation energies between SeaLL1 and experiment for 606 even-even nuclei: $S_{2p}(Z)$ for constant N (a) and $S_{2n}(N)$ for constant Z (b) chains connected by lines.

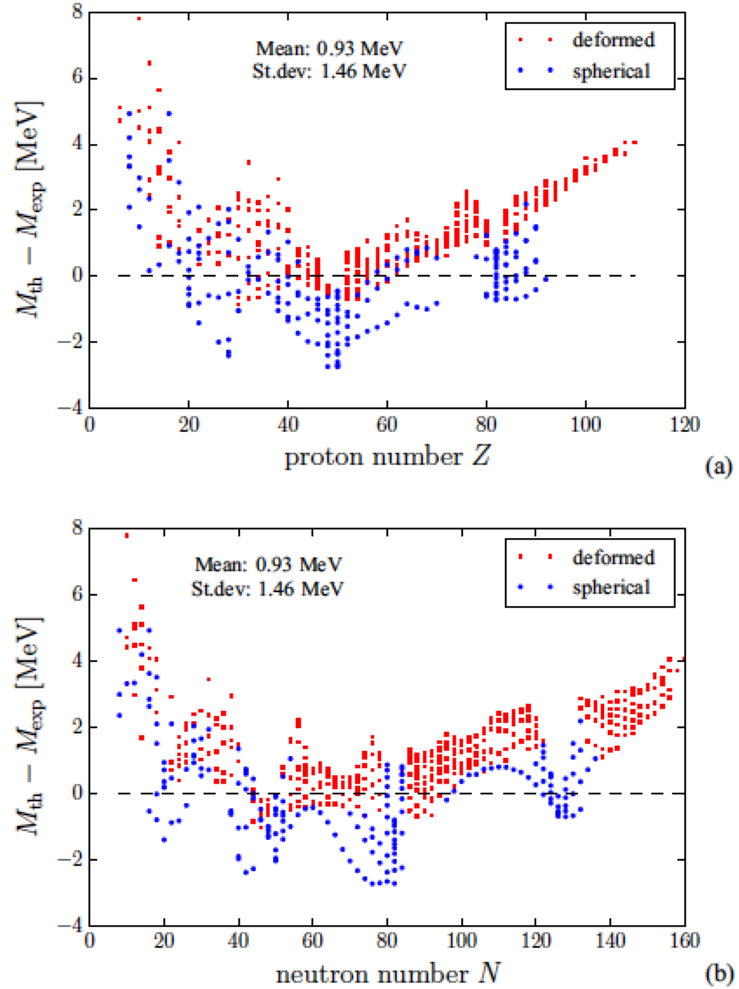

FIG. 8. Mass residuals between SeaLL1 and measured masses for 606 even-even nuclei, of which 410 are deformed nuclei and 196 are spherical nuclei, plotted with red squares and blue bullets respectively as a function of proton number Z (a) and neutron number N (b).

Introducing the center-of-mass correction for spherical nuclei alone reduce the χ_E for the binding energies from 1.54 MeV to 0.97 MeV.
For spherical nuclei one needs also zero-point energy corrections.

Charge radii and charge distributions

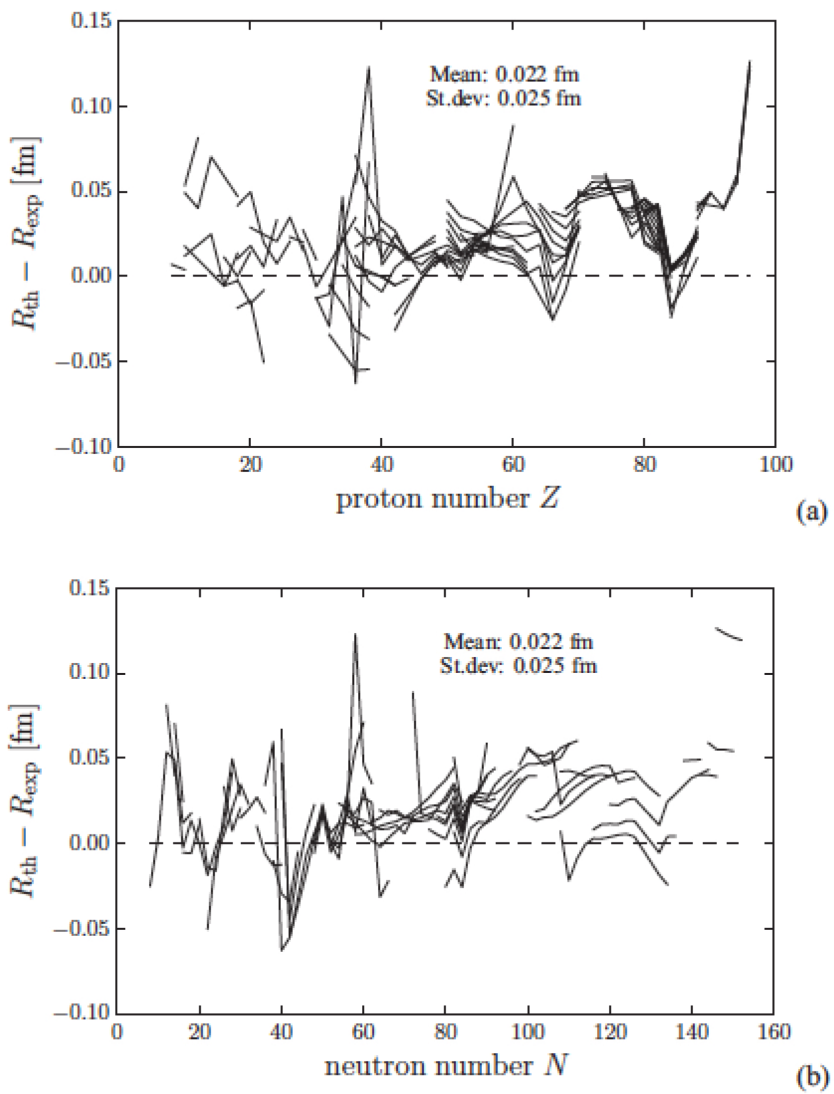

FIG. 12. Radii residuals between SeaLL1 and experiment for 345 even-even nuclei. Isotonic (a) and isotopic (b) chains are connected by lines.

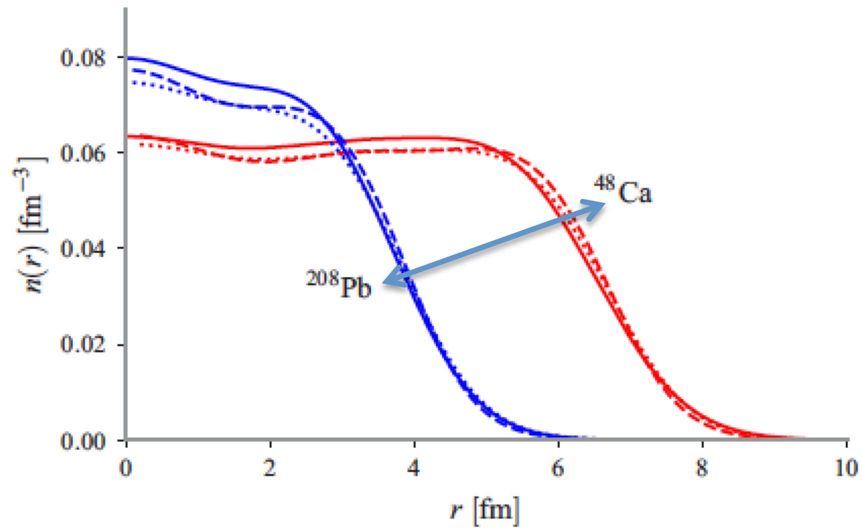

FIG. 11. The calculated proton $n_p(r)$ (dashed) and charge $n_{ch}(r)$ (dotted) densities for ^{48}Ca (red) and ^{208}Pb (blue), calculated with SeaLL1 compared to charge densities (solid) extracted from electron scattering experiments [157].

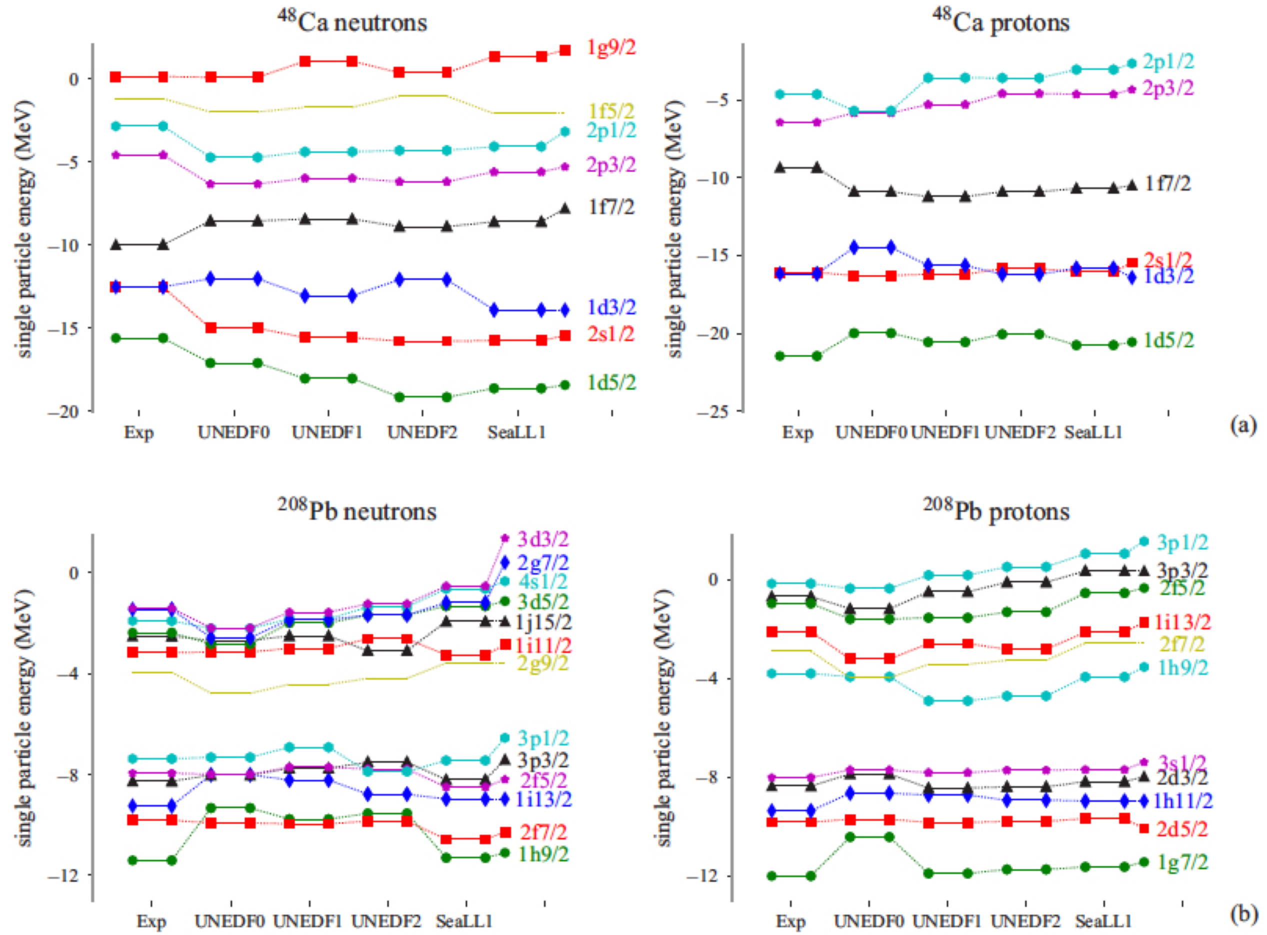

FIG. 13. Single particle energies in ^{48}Ca (a) and ^{208}Pb (b) for a variety of functionals UNEDF0-2 [73–75] and SeaLL1 (calculated using the HFBTHO DFT solver [154]).

^{48}Ca: rms deviations for UNEDF0, UNEDF1, UNEDF2, and SeaLL1 for neutrons/protons: 1.50/1.22, 1.71/1.08, 1.92/1.22, 1.88/1.17 MeV

^{208}Pb: rms deviations for UNEDF0, UNEDF1, UNEDF2, and SeaLL1 for neutrons/protons: 0.82/0.77, 0.61/0.49, 0.69/0.50, 0.62/0.54 MeV

UNEDF2 was constrained to describe single-particle properties too!

Fission pathways

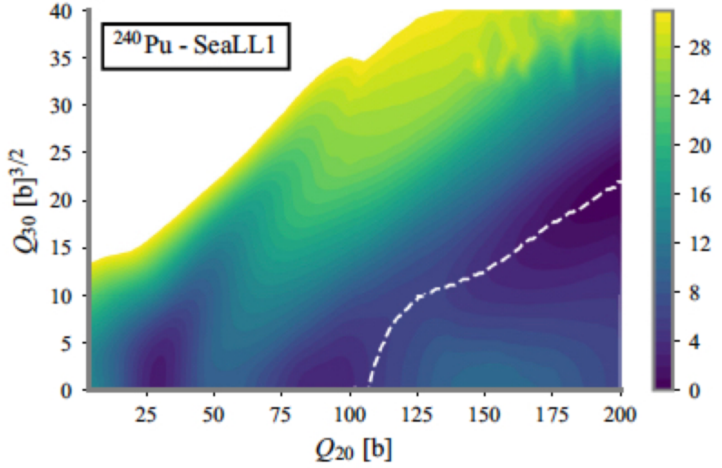

FIG. 14. Two-dimensional potential energy surface of ^{240}Pu with SeaLL1 for $0 \leqslant Q_{20} \leqslant 200$ b, $0 \leqslant Q_{30} \leqslant 40$ b$^{3/2}$. The least-energy fission path is marked as white dashed line.

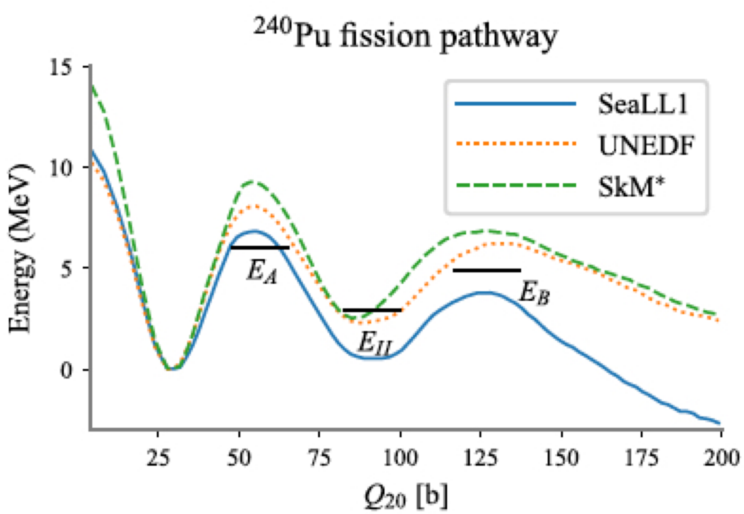

FIG. 15. Fission pathway for ^{240}Pu along the mass quadrupole moment Q_{20} calculated using HFBTHO with SeaLL1, SkM*, and UNEDF1-HFB.

PHYSICAL REVIEW C **89**, 054314 (2014)

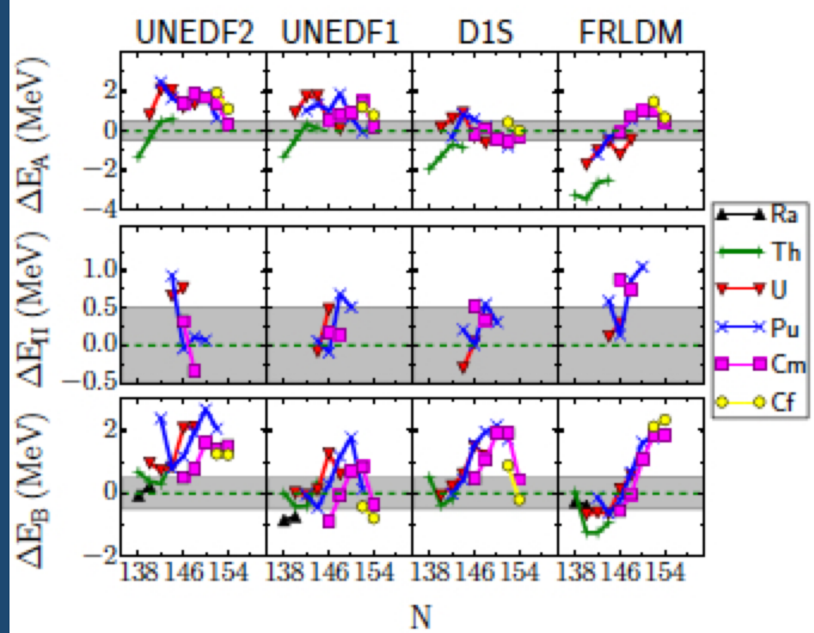

FIG. 12. (Color online) The residuals of the inner fission barriers, ΔE_A, panels (a)–(d); fission isomer excitation energies, ΔE_{II}, panels (e)–(h); and outer fission barriers, ΔE_B, panels (i)–(l), for various actinide nuclei. Residuals are defined as the difference between the computed values with UNEDF2, UNEDF1, D1S, and FRLDM models and the empirical values [83,84]. The shaded area represents an average experimental uncertainty for each quantity.

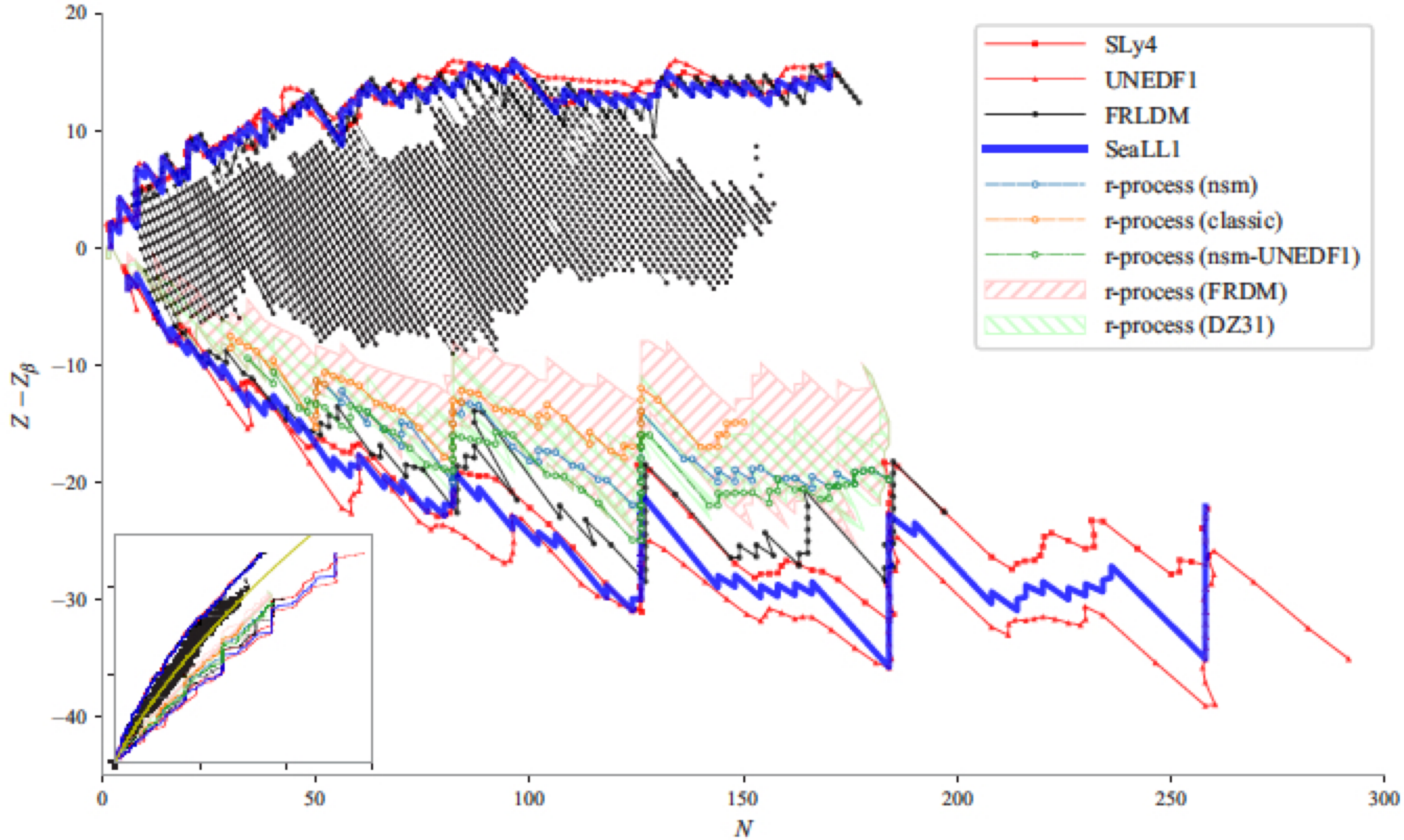

FIG. 16. Fully self-consistent calculations of the proton and neutron driplines for the SeaLL1 NEDF (thick blue line) compared with predictions of the functionals SLy4 and UNEDF1 extracted from Ref. [169], and FRLDM [66]. The vertical axis is shifted by the approximate β-stability line $Z_\beta(N)$ which minimizes Eq. (1) at constant A with parameters from Table I: $\partial_Z E(A-Z,Z)|_{Z=Z_\beta} = 0$, $Z_\beta = A/(2 + a_C A^{2/3}/2a_I)$. The inset shows the usual Z vs N plot, with the $Z = Z_\beta(N)$ curve as a solid (yellow) line. The 2375 nuclear masses from Refs. [18,19] are displayed as dots. We have plotted possible r-process trajectories predicted to be realized in the case of two neutron star mergers [16,17] (red circles), in a classical hot $(n,\gamma) \leftrightarrow (\gamma,n)$ in equilibrium r-process [170] (green circles) with the FRDM model [66] and neutron star merger with the UNEDF1 functional [74] (blue circles). With pink and green bands we display the r-process paths obtained by Mendoza-Temis *et al.* [171] under various conditions using the FRDM model [66] and the Duflo-Zuker model [172].

Pasta phase properties of the neutron star crust as a function of baryon density, evaluated in simulation boxes of various volumes: $32^3 \ldots 96^3$ fm^3

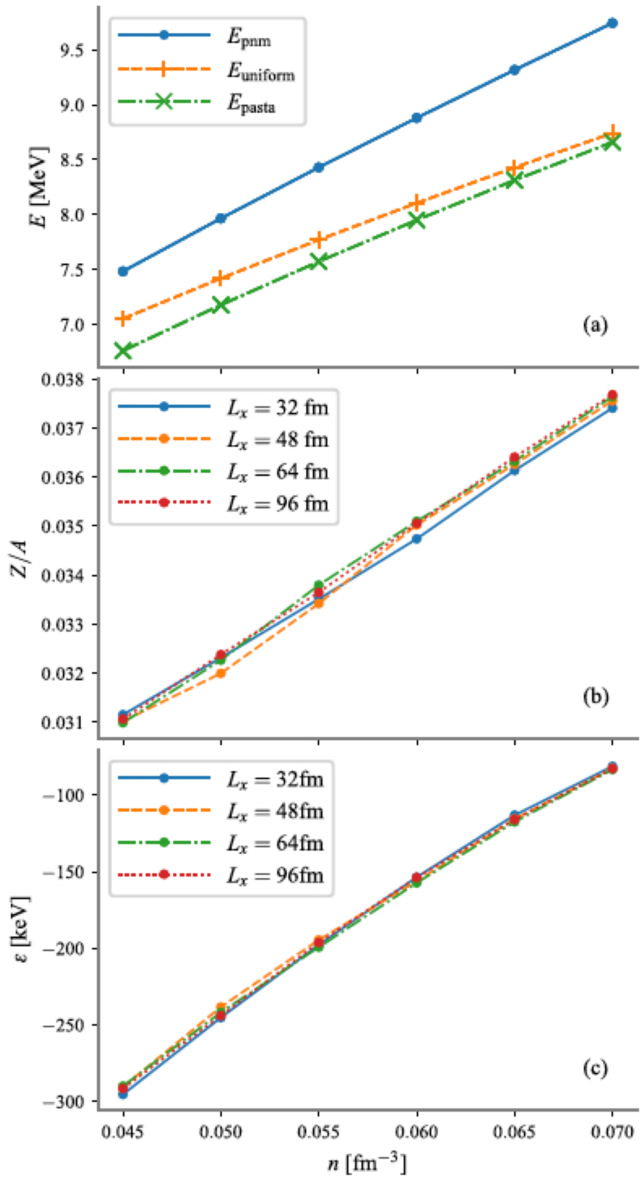

FIG. 17. (a) Energy per baryon in the pasta phase ($E_{\rm past}$), energy per neutron in pure neutron matter ($E_{\rm pnm}$), and energy per baryon in uniform nuclear matter ($E_{\rm uni}$) as a function of average baryon density. (b) Charge ratio of the nuclear pasta as a function of average baryon density. (c) The energy per nucleon difference between the uniform and the inhomogeneous matter configurations in β equilibrium as a function of the average baryon density.

Perspectives

- By introducing two surface terms one can adjust the neutron thickness independently of the symmetry energy properties and one can also control the static electric polarizability. In SeaLL1 $\eta_0 = \eta_1$ and global properties are very weakly dependent on their difference.

$$\mathcal{E}_{\nabla n} = \eta_0 \frac{\hbar^2}{2m} |\nabla n_n + \nabla n_p|^2 + \eta_1 \frac{\hbar^2}{2m} |\nabla n_n - \nabla n_p|^2$$

- One can introduce an isospin dependence of the spin-orbit interaction and control separately the neutron and proton single-particle spectra. In SeaLL1 $W_0 = W_1$ and global properties are very weakly dependent on their difference.

$$\mathcal{E}_{\mathrm{SO}} = W_0 \boldsymbol{J} \cdot \nabla n + W_1 (\boldsymbol{J}_n - \boldsymbol{J}_p) \cdot (\nabla n_n - \nabla n_p),$$

- One can tune the neutron and proton effective masses

$$\mathcal{E}_\tau \propto \tau n^\sigma - j^2 n^{\sigma-1} - \frac{3}{5}(3\pi^2)^{2/3} n^{5/3+\sigma} \propto \frac{|\nabla n|^2}{n^{1-\sigma}}.$$

Perspectives (continued)

- Many modern NEDFs have stronger pairing coupling for protons than for neutrons. This violates isospin symmetry, when not accounting for the role of Coulomb interaction. Coulomb interaction makes the proton pairing weaker. A good choice of the effective coupling constants is
  $g_{eff} < 0$ and $h_{eff} > 0$.

$$\mathcal{E}_\Delta = \int d^3r\; g_{\text{eff}}(\boldsymbol{r})(|\nu_n(\boldsymbol{r})|^2 + |\nu_p(\boldsymbol{r})|^2) + \int d^3r\; h_{\text{eff}}(\boldsymbol{r})(|\nu_n(\boldsymbol{r})|^2 - |\nu_p(\boldsymbol{r})|^2)\beta,$$

$$g(n_n(\boldsymbol{r}), n_p(\boldsymbol{r})) = g(n_p(\boldsymbol{r}), n_n(\boldsymbol{r})),$$
$$h(n_n(\boldsymbol{r}), n_p(\boldsymbol{r})) = h(n_p(\boldsymbol{r}), n_n(\boldsymbol{r})).$$

- Entrainment terms

$$\mathcal{E}_{\text{entrain}} = g_{\text{ent}}\left(\frac{n_n n_p}{n^2}\right)\frac{n}{2m}\left|\frac{\boldsymbol{j}_n}{n_n} - \frac{\boldsymbol{j}_p}{n_p}\right|^2,$$

This term vanishes in the ground state. With this term one can control the isovector giant resonances properties (energy, sum rule).

$$x + g_{\text{ent}}(x) > 0.$$

$$\tilde{\mathcal{E}}_{\text{spin entrain}} = \tilde{g}_{\text{ent}}\left(\frac{n_n n_p}{n^2}\right)\frac{n}{2m}\left|\frac{\boldsymbol{J}_n}{n_n} - \frac{\boldsymbol{J}_p}{n_p}\right|^2,$$

With this term one can control the Gamow-Teller and beta transitions.

- Odd and odd-odd nuclei

$$\tilde{\mathcal{E}}_{\text{spin}} = \alpha_1(\boldsymbol{s}_n^2 + \boldsymbol{s}_p^2) + \alpha_2 \boldsymbol{s}_n \cdot \boldsymbol{s}_p$$

$$\int d^3\boldsymbol{r}\; n_{n,p}(\boldsymbol{r}) \gg \left|\int d^3\boldsymbol{r}\; \boldsymbol{s}_{n,p}(\boldsymbol{r})\right|$$

Important for beta-decay matrix elements

Conclusions

- ✓ This un-optimized NEDF SeaLL1 is physically intuitive and at the present level provides one of the most accurate descriptions of global nuclear properties (masses, charge radii, two-nucleon separation energies, single-particle spectra, etc.) with a surprisingly small number of parameters (seven).
- ✓ The outlined framework provides a clear strategy for further improving the quality of NEDF.
- ✓ We have identified a significant number of parameters, which have little or no influence on the ground state properties. These additional parameters can be used to refine various nuclear properties.

  - Single-particle spectra
  - Static dipole polarizability
  - Neutron skin thickness
  - Symmetry energy properties
  - Isovector giant resonance properties
  - Gamow-Teller and beta transitions
  - Nuclear compressibility and monopole giant resonances
  - Pairing properties